Available online at www.sciencedirect.com
SCIENCE DIRECT®
International Journal of Heat and Mass Transfer 48 (2005) 2896–2910
International Journal of HEAT and MASS TRANSFER
www.elsevier.com/locate/ijhmt

Conjugate forced convection heat transfer from a flat plate by laminar plane wall jet flow

P. Rajesh Kanna, Manab Kumar Das *

Department of Mechanical Engineering, Indian Institute of Technology Guwahati, North Guwahati, Guwahati 781 039, Assam, India

Received 14 July 2004; received in revised form 1 November 2004
Available online 19 April 2005

Abstract

An analytical solution is investigated for forced convection heat transfer from a laminar plane wall jet as conjugate case. For $Re \gg 1$, boundary layer theory is used for the investigation. The problem has been solved for two classic cases such as $Pr \geqslant 1$ and $Pr \ll 1$. The conjugate model consists of considering the full Navier–Stokes equation in the fluid medium and coupling of energy equations in the fluid and the slab through the interface boundary conditions. Closed-form relations are found for Nusselt number (Nu), average Nusselt number ($\overline{Nu}$) and conjugate interface boundary temperature (θ_b). The effects of the Reynolds number (Re), the Prandtl number (Pr), the thermal conductivity ratio (k) between the slab and the fluid medium and the slab aspect ratio (λ) are investigated on the heat transfer characteristics. The analytical results are compared with the full numerical results.

Keywords: Plane wall jet; Conjugate heat transfer; Computation

1. Introduction

A conjugate heat transfer problem occurs when the fluid regime is coupled with the conducting solid wall of finite thickness. The temperature and the heat fluxes at the solid-fluid interface are considered to be equal. This is referred to as the fourth-kind boundary condition [1]. Conjugate heat transfer is involved in many applications like high speed jet engines, electronics cooling, film cooling of turbine blades, extrusion of materials, etc.

Many publications are devoted to conjugate heat transfer on flat plate [2–6]. Chiu et al. [7] studied conjugate heat transfer of horizontal channel both experimentally and numerically. They showed the effects of conjugate heat transfer with non-conjugate results. Rao et al. [8] presented the results for laminar mixed convection with surface radiation from a vertical plate with a heat source as conjugate case. Jilani et al. [9] have solved conjugate heat transfer from a heat generating vertical cylinder.

Glauert [10] defined plane wall jet as a stream of fluid blown tangential along a plane wall. Similarity solution for plane wall jet as well as radial wall jet for both laminar and turbulent cases were presented with the introduction of Glauert constant 'F'. Schwarz and Caswell [11] have investigated the heat transfer characteristics of a two-dimensional laminar incompressible wall jet. They found exact solutions for both constant wall temperature and constant heat flux cases. In addition, they have solved for variable starting length of the heated

* Corresponding author. Tel.: +91 361 2582 655; fax: +91 361 269 0762.
E-mail address: manab@iitg.ernet.in (M.K. Das).

0017-9310/$ - see front matter © 2005 Elsevier Ltd. All rights reserved.
doi:10.1016/j.ijheatmasstransfer.2005.01.033

Nomenclature

A	constant
a	thickness of the slab, m
b	length of the slab, m
h	inlet slot height, m
i	x-direction grid point
j	y-direction grid point
k_f	thermal conductivity of the fluid, W/m K
k_s	thermal conductivity of the slab, W/m K
k	thermal conductivity ratio, k_s/k_f
Nu	local Nusselt number
$\overline{Nu}$	average Nusselt number
n	normal direction
Pr	Prandtl number, $\frac{\nu}{\alpha}$
Q	constant
Re	Reynolds number for the fluid
T_c	constant bottom wall temperature, °C
T_∞	constant ambient temperature, °C
t	non-dimensional time
u, v	dimensional velocity components along (x, y) axes, m/s
$\hat{u}, \hat{v}$	dimensionless velocity components along (x, y) axes
$\bar{u}$	inlet mean velocity, m/s
U_∞	ambient velocity of fluid, m/s
x, y	dimensional Cartesian co-ordinates along and normal to the plate, m
$\hat{x}, \hat{y}$	dimensionless Cartesian co-ordinates $(x, y)/b$

Greek symbols

α	thermal diffusivity, m^2/s
γ	constant
ΔT	temperature difference, $T_c - T_\infty$, °C
ε	convergence criterion
ζ	similarity variable
θ_0	constant
$\bar{\theta}_b$	dimensionless average boundary temperature
θ_b	dimensionless boundary temperature
θ_s	dimensionless temperature in the solid wall
κ	clustering parameter
λ	aspect ratio a/b
ν	kinematic viscosity, m^2/s
σ	dimensionless constant
τ	dimensionless constant
χ	constant
ψ	dimensionless stream function
ω	dimensionless vorticity

Subscripts

b	interface
f	fluid
s	solid
w	wall
∞	ambient condition

section at constant wall temperature. The solution was derived with the plate and jet regimes as non-conjugated. Angirasa [12] has studied laminar buoyant wall jet and reported the effect of velocity and the width of the jet during convective heat transfer from the vertical surface.

Amitay and Cohen [13] have reported the effects of wall blowing and suction on the stability characteristics of a laminar incompressible two-dimensional plane wall jet. Cohen et al. [14] did work on transition of wall jets subjected to blowing and suction. Quintana et al. [15] experimentally investigated the mean and fluctuating characteristics of a plane unsteady laminar wall jet for constant wall temperature. Seidel [16] has done numerical work to find the effect of high amplitude forcing on laminar and turbulent wall jet over a heated flat plate. Seidel has used DNS for laminar case and RANS for turbulent wall jet. Recently, Bhattacharjee and Loth [17] simulated laminar and transitional cold wall jets. They investigated the significance of three different inlet profiles viz. parabolic, uniform and ramp. They presented the detailed results of time-averaged wall jet thickness and temperature distribution with RANS approach for higher Reynolds number and DNS approach for three-dimensional wall jet. Vynnycky et al. [6] have presented an analytical solution of two-dimensional conjugate heat transfer problem of laminar boundary layer over a flat plate for both high Pr as well as low Pr. They have validated their analytical results with the numerical results.

The present study is motivated by the cooling of heated slabs due to laminar plane wall jet flow. These type of conjugate heat transfer situations are found in electronics cooling, refrigerated air curtain, paper industry, electrical motor cooling, etc. Here, a conjugate heat transfer by a two-dimensional laminar plane wall jet flow over a solid slab has been considered. An analytical solution has been presented for $Pr \ll 1$ and $Pr \geqslant 1$ cases with k, Re and λ as the parameters. The analytical solution has been compared and validated with a numerical solution. For this purpose, the problem has also been solved numerically with stream function-vorticity method considering it to be an unsteady-state formulation. The integration in time has been allowed till a steady-state solution is obtained.

2. Basic equations

Consider the steady two-dimensional heat transfer over a rectangular slab of finite thickness. A jet of fluid strikes the wall, which is submerged in the same fluid thus developing wall jet. A schematic representation of the domain is shown in Fig. 1. The slab thickness is $-a \leqslant y \leqslant 0$ and the length is $\frac{-b}{2} \leqslant x \leqslant \frac{b}{2}$. The fluid has uniform temperature and velocity at inlet (i.e. $x = -\frac{1}{2}$). The bottom of the wall is maintained at constant temperature, $T_c > T_\infty$. The other ends of the wall are thermally insulated. It is assumed that the temperature gradient of solid wall in axial direction is negligible while comparing temperature gradient in normal direction, which is consistent with boundary layer theory. The surrounding of the fluid is assumed as quiescent regime. Following non-dimensional variables are used to express the problem.

$$\hat{x} = \frac{x}{b}, \quad \hat{y} = \frac{y}{b}, \quad \hat{u} = \frac{u}{U_\infty}\frac{1}{\sqrt{Re}}, \quad \hat{v} = \frac{v}{U_\infty}\frac{1}{\sqrt{Re}},$$
$$\hat{\psi} = \frac{\psi}{bU_\infty}, \quad \hat{\omega} = \frac{b\omega}{U_\infty}\frac{1}{\sqrt{Re}}, \quad \hat{\theta}_f = \frac{T_f - T_\infty}{\Delta T}, \quad \hat{\theta}_s = \frac{T_s - T_\infty}{\Delta T}, \tag{1}$$

where $\Delta T = T_c - T_\infty$ and ψ is the stream function which is defined by

$$u = \frac{\partial \psi}{\partial y}, \; v = -\frac{\partial \psi}{\partial x} \tag{2}$$

The equations governing the vorticity and energy transport for the fluid (dropping the hats for all the variables for clarity)

$$\nabla^2 \psi = -\omega \tag{3a}$$

$$u\frac{\partial \omega}{\partial x} + u\frac{\partial \omega}{\partial y} = \frac{1}{Re^{3/2}}\nabla^2 \omega \tag{3b}$$

$$u\frac{\partial \theta_f}{\partial x} + u\frac{\partial \theta_f}{\partial y} = \frac{1}{Pr\,Re^{3/2}}\nabla^2 \theta_f \tag{3c}$$

and for the conductive slab

$$\nabla^2 \theta_s = 0 \tag{3d}$$

where ∇^2 is the Laplacian in Cartesian co-ordinates (x, y). The boundary conditions for Eqs. (3a)–(3d) are

$$\psi = \frac{\partial \psi}{\partial y} = 0 \quad \text{on } y = 0 \quad |x| \leqslant \frac{1}{2} \tag{4a}$$

$$\theta_s = \theta_f = 0 \quad \text{on } y = 0 \quad |x| \leqslant \frac{1}{2} \tag{4b}$$

$$\frac{\partial \theta_f}{\partial y} = k\frac{\partial \theta_s}{\partial y} \quad \text{on } y = 0 \quad |x| \leqslant \frac{1}{2} \tag{4c}$$

$$\frac{\partial \theta_s}{\partial y} = 0 \quad \text{on } x = \pm\frac{1}{2} \quad -\lambda \leqslant y \leqslant 0 \tag{4d}$$

$$\theta_s = 1 \quad \text{on } y = -\lambda \quad |x| \leqslant \frac{1}{2} \tag{4e}$$

$$\theta_f \to 0 \quad \text{as } y \to \infty \quad |x| \leqslant \frac{1}{2} \tag{4f}$$

$$\frac{\partial \psi}{\partial y} \to 0 \quad \text{as } y \to \infty \quad |x| \leqslant \frac{1}{2} \tag{4g}$$

$$\omega \to 0 \quad \text{as } y \to \infty \quad |x| \leqslant \frac{1}{2} \tag{4h}$$

The local Nusselt number is

$$Nu = -\left(\frac{\partial \theta_f}{\partial y}\right)_{y=0}, \quad |x| \leqslant \frac{1}{2} \tag{5}$$

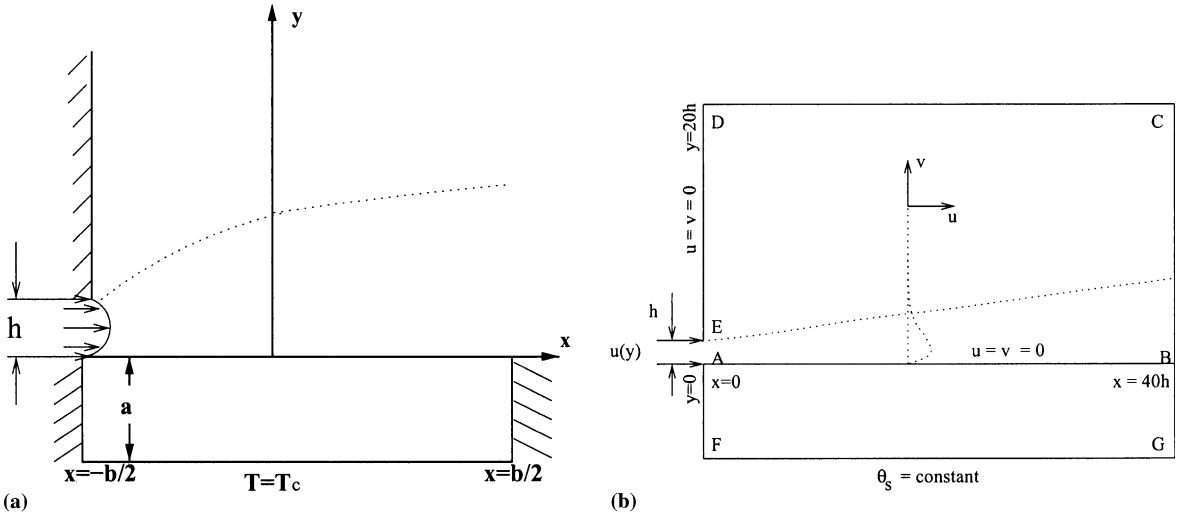

Fig. 1. Combination of a wall jet with solid wall: (a) schematic diagram and (b) coordinate system and boundary condition.

The average Nusselt number is defined as

$$\overline{Nu} = \int_{-1/2}^{1/2} Nu\,\mathrm{d}x \tag{6}$$

While finding out the closed form solution for the energy equation, it is mandatory to obtain the similarity solution for the momentum equation. The solution proceeded for two classical cases such as Pr approaches infinity and Pr approaches zero. Pr number is the ratio of momentum transport property and thermal transport property of fluid in forced convection heat transfer [18]. For high Pr fluid, the thermal boundary layer thickness is smaller than viscous boundary layer thickness and vice versa. For $Pr \ll 1$, the viscous boundary layer can be ignored while calculating thermal boundary layer. Whereas for $Pr \geqslant 1$, within the thermal boundary layer region velocity depends on y. Liquid metals come under the family of $Pr \ll 1$ while oils are having $Pr \geqslant 1$. If the non-dimensional temperature at entry of slab fluid interface $(-1/2,0)$ is denoted as θ_0, then its value varies from 0 to 1. When $\theta_0 = 0$, heat is transferred to the flow at leading edge which is a singular point. This is valid for $Pr \geqslant 1$ and $Pr \ll 1$.

$Pr \geqslant 1$

Case I: For $\theta_0 > 0$ the suitable scalings are

$$\psi = Re^{-3/4}\Psi, \quad \omega = Re^{3/4}\Omega, \quad y = Re^{-3/4}Y \tag{7}$$

With this new scalings, Eqs. (3a)–(3c) become

$$\frac{\partial^2 \Psi}{\partial Y^2} = -\Omega \tag{8a}$$

$$\frac{\partial \Psi}{\partial Y}\frac{\partial \Omega}{\partial X} - \frac{\partial \Psi}{\partial X}\frac{\partial \Omega}{\partial Y} = \frac{\partial^2 \Omega}{\partial Y^2} \tag{8b}$$

$$Pr\left(\frac{\partial \Psi}{\partial Y}\frac{\partial \theta_f}{\partial X} - \frac{\partial \Psi}{\partial X}\frac{\partial \theta_f}{\partial Y}\right) = \frac{\partial^2 \theta_f}{\partial Y^2} \tag{8c}$$

From Eqs. (8a) and (8b),we eliminate Ω and integrate once with respect to Y to obtain

$$\frac{\partial \Psi}{\partial Y}\frac{\partial^2 \Psi}{\partial X \partial Y} - \frac{\partial \Psi}{\partial X}\frac{\partial^2 \Psi}{\partial Y^2} = \frac{\partial^3 \Psi}{\partial Y^3} \tag{9}$$

where $X = x + 1/2$. The boundary layer begins at $X = 0$. The boundary conditions relevant to the above equations are

$$\Psi = \frac{\partial \Psi}{\partial Y} = 0 \quad \text{on } Y = 0 \quad X \geqslant 0 \tag{10a}$$

$$\theta_f = \theta_s \quad \text{on } Y = 0 \quad 0 \leqslant X \leqslant 1 \tag{10b}$$

$$\frac{\partial \theta_f}{\partial Y} = \frac{1}{\sigma}\frac{\partial \theta_s}{\partial y} \quad \text{on } Y = 0 \quad 0 \leqslant X \leqslant 1 \tag{10c}$$

where $\sigma = \frac{Re^{3/4}}{k}$ is a dimensionless parameter. Since uniform stream at ambient temperature is passing through the inlet slot, appropriate conditions at entry are

$$\frac{\partial \Psi}{\partial Y} = 1 \quad \text{at } X = 0 \tag{11a}$$

$$\theta_f = 0 \quad \text{as } X = 0 \tag{11b}$$

To evaluate the analytical solution, we transform the basic Eqs. (9)–(11b) using similarity variable of Glauert [10]

$$\Psi = X^{1/4}F(X,\zeta), \quad \zeta = \frac{Y}{4X^{3/4}}, \quad \theta_f(X,Y) = G(X,\zeta) \tag{12}$$

Eqs. (9) and (8c) are reduced to

$$F''' + 2F'^2 + FF'' = 4X\left(F'\frac{\partial F'}{\partial X} - F''\frac{\partial F}{\partial X}\right) \tag{13a}$$

$$\frac{G''}{Pr} + FG' = 4X\left(F'\frac{\partial G}{\partial X} - G'\frac{\partial F}{\partial X}\right) \tag{13b}$$

where the prime denotes differentiation with respect to ζ. The boundary conditions in terms of F and G are

$$F = F' = 0 \quad \text{on } \zeta = 0 \tag{14a}$$

$$\theta_s = G \quad \text{on } \zeta = 0 \tag{14b}$$

$$\frac{\partial \theta_s}{\partial y} = \frac{1}{4X^{3/4}}\sigma G' \quad \text{on } \zeta = 0 \tag{14c}$$

$$F' \to 0, \; G \to 0 \quad \text{as } \zeta \to \infty \tag{14d}$$

Let $X \to 0$, and we arrive at the ordinary differential equations

$$F''' + 2F'^2 + FF'' = 0 \tag{15a}$$

$$\frac{G''}{Pr} + FG' = 0 \tag{15b}$$

subject to

$$F = F' = 0 \quad \text{on } \zeta = 0 \tag{16a}$$

$$F' \to 0, \; G \to 0 \quad \text{as } \zeta \to \infty \tag{16b}$$

with the Eq. (14b) replaced as

$$G = \theta_0 \quad \text{on } \zeta = 0 \tag{16c}$$

It is observed that the continuity of heat flux at interface at $X = 0$, further the canonical substitution $G = \theta_0 \widehat{G}$ the Eq. (14c) becomes

$$\frac{\partial \theta_s}{\partial y} = \frac{1}{4X^{3/4}}\sigma\theta_0\widehat{G}'(0) \tag{17}$$

The heat flux has singularity at $X \to 0$. We remove it using plane polar coordinates (r,ϕ) as follows,

$$X = r\cos\phi \quad y = r\sin\phi$$

The boundary conditions (4d) and (17) become,

$$\frac{\partial\theta_s}{\partial\phi}=0 \quad \text{on } \phi=-\frac{\pi}{2} \tag{18a}$$

$$\frac{\partial\theta_s}{\partial\phi}=\frac{1}{4}\sigma\theta_0\widehat{G}'(0)r^{1/4} \quad \text{on } \phi=0 \tag{18b}$$

A harmonic function which satisfies these boundary condition is

$$\hat{\theta}_s(r,\phi)=Ar^{1/4}\sin\frac{\phi}{2} \tag{19}$$

where

$$A=-\frac{1}{\sqrt{2}}\sigma\theta_0\widehat{G}'(0) \tag{20}$$

The singularity at $r=0$ is removed by defining $\theta_s=\hat{\theta}_s+\theta_s^*$. So θ_s^* satisfies

$$\nabla^2\theta_s^*=0 \tag{21}$$

subject to

$$\theta_s^*=\theta_0\widehat{G}-\hat{\theta}_s \quad y=0 \quad 0\leqslant X\leqslant 1 \tag{22a}$$

$$\frac{\partial\theta_s^*}{\partial y}=\frac{\sigma\theta_0\widehat{G}'}{4X^{3/4}}-\frac{\partial\hat{\theta}_s}{\partial y} \quad \text{on } y=0 \quad 0\leqslant X\leqslant 1 \tag{22b}$$

$$\frac{\partial\theta_s^*}{\partial X}=0 \quad \text{on } X=0 \quad -\lambda\leqslant y\leqslant 0 \tag{22c}$$

$$\frac{\partial\theta_s^*}{\partial X}=-\frac{\partial\hat{\theta}_s}{\partial y} \quad \text{on } X=1 \quad -\lambda\leqslant y\leqslant 0 \tag{22d}$$

$$\theta_s^*=1-\hat{\theta}_s \quad \text{on } y=-\lambda \quad 0\leqslant X\leqslant 1 \tag{22e}$$

Case II: For the case $\theta_0=0$, the similarity variables have small changes as follows

$$\Psi=X^{1/4}F(X,\zeta), \quad \theta_f=X^{3/4}G(X,\zeta), \quad \zeta=\frac{Y}{4X^{3/4}} \tag{23}$$

The basic governing equations become

$$F'''+2F'^2+FF''=4X\left(F'\frac{\partial F'}{\partial X}-F''\frac{\partial F}{\partial X}\right) \tag{24a}$$

$$\frac{G''}{Pr}+FG'-3F'G=4X\left(F'\frac{\partial G}{\partial X}-G'\frac{\partial F}{\partial X}\right) \tag{24b}$$

subject to the boundary conditions for $0\leqslant X\leqslant 1$

$$F=F'=0 \quad \text{on } \zeta=0 \tag{25a}$$

$$\theta_s=X^{3/4}G \quad \text{on } \zeta=0 \tag{25b}$$

$$\frac{\partial\theta_s}{\partial y}=\frac{\sigma G'}{4X^{3/4}} \quad \text{on } \zeta=0 \tag{25c}$$

$$F'\to 0, \quad G\to 0 \quad \text{as } \zeta\to\infty \tag{25d}$$

Let $X\to 0$. Eqs. (24a) and (24b) become

$$F'''+FF''+2F'^2=0 \tag{26a}$$

$$\frac{G''}{Pr}+FG'-3F'G=0 \tag{26b}$$

subject to

$$F=F'=0 \quad \text{on } \zeta=0 \tag{27a}$$

$$F'\to 0, \quad G\to 0 \quad \text{as } \zeta\to\infty \tag{27b}$$

Eqs. (26a) and (26b) are same as the expressions given by Schwarz and Caswell [11].

An extra boundary condition is availed for being canonical forms $G=Q\widehat{G}$ as solutions to above equations. The unknown constant Q can be found from the continuity of heat flux at $Y=0$ from the solution of θ_s.

Now the boundary conditions are

$$\widehat{G}'(0)=-1 \tag{28a}$$

$$\theta_s=X^{3/4}Q\widehat{G} \quad \text{on } y=0 \quad 0\leqslant X\leqslant 1 \tag{28b}$$

$$\frac{\partial\theta_s}{\partial y}=\frac{1}{4}\sigma\widehat{G}'Q \quad \text{on } y=-\lambda \quad 0\leqslant X\leqslant 1 \tag{28c}$$

$$\theta_s=1 \quad \text{on } y=0 \quad 0\leqslant X\leqslant 1 \tag{28d}$$

$$\frac{\partial\theta_s}{\partial X}=0 \quad \text{on } X=1,\ 0 \quad -\lambda\leqslant y\leqslant 0 \tag{28e}$$

$Pr\ll 1$

For lower Prandtl number the thermal boundary layer thickness is higher than viscous boundary layer. According to this, change in scaling is done in y coordinate only and is given by,

$$y=Pr^{-1}Re^{-3/4}Y$$

The boundary layer equations for fluid field are now

$$\frac{\partial\Psi}{\partial Y}\frac{\partial^2\Psi}{\partial Y\partial X}-\frac{\partial\Psi}{\partial X}\frac{\partial^2\Psi}{\partial Y^2}=0 \tag{29a}$$

$$\frac{\partial\Psi}{\partial Y}\frac{\partial\theta_f}{\partial X}-\frac{\partial\Psi}{\partial X}\frac{\partial\theta_f}{\partial Y}=\frac{\partial^2\theta_f}{\partial Y^2} \tag{29b}$$

From the above, one obtains

$$\Psi\equiv Y \tag{30a}$$

$$\frac{\partial\theta_f}{\partial X}=\frac{\partial^2\theta_f}{\partial Y^2} \tag{30b}$$

subject to

$$\theta_f=\theta_s \quad \text{on } Y=0 \quad 0\leqslant X\leqslant 1 \tag{31a}$$

$$\frac{\partial\theta_s}{\partial y}=\sigma\frac{\partial\theta_f}{\partial Y}\quad \text{on } Y=0\quad 0\leqslant X\leqslant 1 \tag{31b}$$

$$\theta_f\ \to\ 0\quad \text{as } Y\ \to\ \infty \tag{31c}$$

$$\theta_f=0\quad \text{at } X=0 \tag{31d}$$

where $\sigma=\frac{Pr\,Re^{3/4}}{k}$. While considering $\theta_0>0$, the discontinuity exists when $\theta_0>0$ at $X=0$, $Y=0$, which is overcome by coordinate transformation as given below.

$$\eta=\frac{Y}{X^{1/2}},\quad S=X^{1/2} \tag{32}$$

From Eqs. (29b) and (30b),

$$\frac{\partial^2\theta_f}{\partial\eta^2}=\frac{1}{2}\left(S\frac{\partial\theta_f}{\partial S}-\eta\frac{\partial\theta_f}{\partial\eta}\right) \tag{33}$$

subject to

$$\theta_s=\theta_f\quad \text{on } \eta=0\quad 0\leqslant S\leqslant 1 \tag{34a}$$

$$\frac{1}{\sigma}\frac{\partial\theta_s}{\partial y}=\frac{1}{S}\frac{\partial\theta_f}{\partial\eta}\quad \text{on } \eta=0\quad 0\leqslant S\leqslant 1 \tag{34b}$$

$$\theta_f\ \to\ 0\quad \text{as } \eta\ \to\ \infty \tag{34c}$$

Now Eq. (31d) is replaced by considering the limits of Eqs. (33), (34a)–(34c) and let $S\to 0$, one obtains an ordinary differential equation

$$\frac{\partial^2\theta_f}{\partial\eta^2}+\frac{\eta}{2}\frac{\partial\theta_f}{\partial\eta}=0 \tag{35}$$

subject to

$$\theta_f\ \to\ 0\quad \text{as } \eta\ \to\ \infty \tag{36a}$$

$$\theta_f=0\quad \text{as } \eta=0 \tag{36b}$$

which leads to solution

$$\theta_f=\theta_0\,\mathrm{erfc}\left(\frac{\eta}{2}\right) \tag{37}$$

The erfc(X) denotes the complementary error function defined by $\mathrm{erfc}(X)=\frac{2}{\sqrt{\pi}}\int_X^\infty e^{-s^2}\,ds$. Subsequently, one arrives at

$$\frac{\partial\theta_s}{\partial y}\sim\frac{\sigma\theta_0}{\sqrt{\pi X}}\quad \text{on } y=0\quad \text{as } X\ \to\ 0 \tag{38}$$

By analogy with Eqs. (17) and (20), one should take

$$A=\frac{1}{\sqrt{2\pi}}\sigma\theta_0 \tag{39}$$

When $\theta_0=0$, there is no singularity at $X=0$, $Y=0$. Considering the solid slab, it is assumed that the axial conduction is negligible compared with normal direction and thus,

$$\frac{\partial^2\theta_s}{\partial y^2}=0 \tag{40}$$

After integrating, one obtains

$$\theta_s(X,y)=\frac{\theta_b(X)-1}{\lambda}y+\theta_b(X) \tag{41}$$

which leads to Eq. (30b) subject to Eqs. (31c) and (31d). The normal direction temperature gradients are balanced at interface, and

$$\frac{\partial\theta_f}{\partial Y}=\tau(\theta_f-1) \tag{42}$$

where $\tau=k/(\lambda Pr\,Re^{3/4})$.

With reference to Carslaw and Jaeger [19], the solution for θ_f for $0\leqslant X\leqslant 1$ can be written as

$$\theta_f(X,Y)=\mathrm{erfc}\left(\frac{\eta}{2}\right)-e^{(\tau Y+\tau^2 X)}\,\mathrm{erfc}\left(\frac{\eta}{2}+\tau\sqrt{X}\right) \tag{43}$$

Setting $Y=0$, the interface temperature is given by,

$$\theta_b=1-e^{\tau^2 X}\,\mathrm{erfc}\,(\tau\sqrt{X}) \tag{44}$$

2.1. Quasi-two-dimensional analogue

To find out the temperature distribution in solid wall, the boundary condition at interface is needed. So the average conjugate boundary temperature and the average Nusselt number are evaluated. The average conjugate boundary temperature, $\bar{\theta}_b$ is defined as

$$\bar{\theta}_b=\int_0^1\theta_b(X,0)\,dX \tag{45}$$

Averaging (41) over $0\leqslant X\leqslant 1$ gives

$$\theta_s(y)=\frac{\bar{\theta}_b-1}{\lambda}y+\bar{\theta}_b \tag{46}$$

Integrating Eq. (14c) over $0\leqslant X\leqslant 1$ and using Eq. (46), one obtains

$$\frac{k}{\lambda}(\bar{\theta}_b-1)=Re^{3/4}\bar{\theta}_b\widehat{G}'(0) \tag{47}$$

where $\widehat{G}'(0)$ depends on Pr only. For large value of Pr, $\widehat{G}'(0)$ are evaluated using *Simpson's one-third rule* numerical integration and approximated value arrived at by least square method as given below.

$$G'(0)=0.3236Pr^{1/3} \tag{48}$$

Rearranging Eq. (47)

$$\bar{\theta}_b=\frac{1}{1+\mu} \tag{49}$$

where

$$\mu=\frac{\lambda}{k}\frac{Pr^{1/3}Re^{3/4}}{3.09} \tag{50}$$

From (4c) and averaging (41) over $0\leqslant X\leqslant 1$, the average Nusselt number is given by

$$\overline{Nu}=\frac{k}{\lambda}\frac{\mu}{(1+\mu)} \tag{51}$$

The case for $Pr \ll 1$ proceeds in a similar way except in place of Eq. (47), the expression is given by

$$\frac{k(\bar{\theta}_b - 1)}{\lambda} = \frac{2}{\sqrt{\pi}} Pr Re^{3/4} \bar{\theta}_b \tag{52}$$

θ_b and $\overline{Nu}$ are same as above except in place of Eq. (50), μ, is given by

$$\mu = \frac{2}{\sqrt{\pi}} \frac{\lambda Pr Re^{3/4}}{k} \tag{53}$$

Since the temperature at interface is non-uniform and the temperature profiles are self-preserving

$$\theta_b(x) = \chi \left(x + \frac{1}{2} \right)^{\gamma} \quad \frac{-1}{2} \leqslant x \leqslant \frac{1}{2} \tag{54}$$

The value of 'γ' is obtained from Schwarz and Caswell [11] and 'χ' is constant flux given by

$$\chi \int_{-1/2}^{1/2} \left(x + \frac{1}{2} \right)^{\gamma} dx = \bar{\theta}_b \tag{55}$$

With known $\bar{\theta}_b$ and $\chi, \theta_b(X)$ can be found. Now the Dirchlet problem for θ_s subject to Eqs. (4d) and (4e) and

$$\theta_s = \theta_b(x) \quad \text{on } y = 0 \quad \frac{-1}{2} \leqslant x \leqslant \frac{1}{2} \tag{56}$$

gives a series form of solution [16]

$$\theta_s(x,y) = \frac{-y}{\lambda} + 2(\gamma+1)\bar{\theta}_b \sum_{n=1}^{\infty} I_n \frac{\sinh n\pi(y+\lambda)}{\sinh n\pi\lambda} \times \cos n\pi \left(x + \frac{1}{2} \right) \tag{57}$$

where, $I_n = \int_0^1 x^{\gamma} \cos n\pi x \, dx$.

The heat flux at the conjugate boundary is then

$$\left(\frac{\partial \theta_s}{\partial y} \right)_{y=0} = \frac{-1}{y} + 2(\gamma+1)\bar{\theta}_b \pi \sum_{n=1}^{\infty} I_n \times \coth n\pi\lambda \cos n\pi \left(x + \frac{1}{2} \right) \tag{58}$$

3. Numerical solution

The unsteady state stream function-vorticity equation governing the incompressible laminar flow in non-dimensional form are (after dropping the hats for the variable)

Stream function equation

$$\nabla^2 \psi = -\omega \tag{59a}$$

Vorticity equation

$$\frac{\partial \omega}{\partial t} + \frac{\partial (u\omega)}{\partial x} + \frac{\partial (v\omega)}{\partial y} = \frac{1}{Re} \nabla^2 \omega \tag{59b}$$

Energy equation

$$\frac{\partial \theta_f}{\partial t} + \frac{\partial (u\theta_f)}{\partial x} + \frac{\partial (v\theta_f)}{\partial y} = \frac{1}{Re\,Pr} \nabla^2 \theta_f \tag{59c}$$

For solid region the energy equation,

$$\frac{\partial \theta_s}{\partial t} - \frac{1}{Re\,Pr} \nabla^2 \theta_s = 0 \tag{59d}$$

where

$$u = \frac{\partial \psi}{\partial y}, \quad v = -\frac{\partial \psi}{\partial x}, \quad Re = \frac{h\bar{u}}{\nu}, \quad Pr = \frac{\nu}{\alpha}$$

The following non-dimensional variables are used for Eqs. (59a)–(59d).

$$\hat{x} = \frac{x}{h}, \quad \hat{y} = \frac{y}{h}, \quad \hat{u} = \frac{u}{\bar{u}}, \quad \hat{v} = \frac{v}{\bar{u}}, \quad \hat{\psi} = \frac{\psi}{h\bar{u}},$$
$$\hat{\omega} = \frac{h\omega}{\bar{u}}, \quad \hat{\theta} = \frac{T - T_\infty}{T_\infty - T_w}, \quad \hat{t} = \frac{t}{h/\bar{u}}.$$

The energy equation in fluid regime and solid regime are solved simultaneously. The slab energy equation is written in transient non-dimensionalised form. The point to note here is that the second term (Eq. (59d)) contains Re and Pr. They appear because of the type of non-dimensionalisation. Similar form of equation has been given by Chiu et al. [7].

The computational domain considered here is clustered Cartesian grids. For unit length, the grid space at ith node is given by the expression [20],

$$x_i = \left(\frac{i}{i_{max}} - \frac{\kappa}{\theta} \sin \left(\frac{i\theta}{i_{max}} \right) \right) \tag{60}$$

$\theta = 2\pi$ stretches both end of the domain whereas $\theta = \pi$ clusters more grid points near one end of the domain. κ varies between 0 and 1. When it approaches 1 more points fall near the end.

The unsteady vorticity transport Eq. (59b) in time is solved by alternate direction implicit scheme (ADI). The central differencing scheme is followed for both the convective as well as the diffusive terms. It is first-order accurate in time and second-order accurate in space $O(\Delta t, \Delta x^2, \Delta y^2)$, and is unconditionally stable. The Poisson Eq. (59a) is solved explicitly by five point Gauss–Seidel methods. Constant time step 0.001 is used for the entire calculation. It has been observed that for coarse grids, larger time step can be used whereas for fine grids, the solution diverges with large time step. While selecting k, time step also needs to be considered. The maximum vorticity error behavior is complicated as explained by Roache [21]. While marching in time for the solution, it has been observed that the maximum vorticity error gradually decreases. It then increases drastically finally decreases asymptotically leading to steady-state solution. The convergence criteria to be set in such a way that it should not terminate at false stage. At steady state, the error reaches the asymptotic

behavior. Here it is set as sum of vorticity error reduced to either the convergence criteria ε or large total time.

$$\sum_{i,j=1}^{i_{\max},j_{\max}} (\omega_{i,j}^{t+\Delta t} - \omega_{i,j}^{t}) < \varepsilon \tag{61}$$

Comini et al. [22] used low *Re* steady-state solution as initial guess value for high *Re* flow for stream function and vorticity. Thom's vorticity condition has been used to obtain the wall vorticity as given below.

$$\omega_{\mathrm{w}} = -\frac{2(\psi_{w+1} - \psi_{\mathrm{w}})}{\Delta n^2} \tag{62}$$

where Δn is the grid space normal to the wall. It has been shown by Napolitano et al. [23] and Huang and Wetton [24] that convergence in the boundary vorticity is actually second-order for steady problems and for time-dependent problems when $t > 0$. Roache [21] has reported that for a Blausius boundary-layer profile, numerical test verify that this first-order form is more accurate than second-order form.

The wall jet consists of an inner region and an outer region. It is a combination of boundary layer flow over flat plate at inner region and plane free jet at outer region [25]. The velocity profile has a point of inflexion. The surrounding medium of wall jet may be quiescent or co-flow or counter-flow depending upon the applications. In the present case, the surrounding is considered to be quiescent.

The inlet slot height $h = 0.5$ is assumed. At the bottom wall and the left side wall, constant stream lines are assumed based on inlet flow. At the outlet in the downstream direction, stream-wise gradients are assumed to be zero. At the entrainment boundary, normal velocity gradient is zero [26]. The detailed boundary conditions are given below (Fig. 1(b)).

$$\text{at AE,}\quad u(y) = 12y - 24y^2;\quad \psi(y) = 6y^2 - 8y^3 \qquad \omega(y) = 48y - 12; \tag{63a}$$

$$\text{along ED,}\quad u = v = 0;\quad \psi = 0.50;\quad \omega = -\frac{2\psi_{\mathrm{w}} - \psi_{w+1}}{\Delta x^2} \tag{63b}$$

$$\text{along AB,}\quad u = v = 0;\quad \psi = 0;\quad \omega = \frac{2\psi_{w+1}}{\Delta y^2} \tag{63c}$$

$$\text{along BC,}\quad \frac{\partial u}{\partial x} = 0;\quad \frac{\partial v}{\partial x} = 0 \tag{63d}$$

$$\frac{\partial^2 \psi}{\partial x^2} = 0;\quad \frac{\partial \omega}{\partial x} = 0 \tag{63e}$$

$$\text{along CD,}\quad \frac{\partial u}{\partial y} = 0 \tag{63f}$$

$$\text{along AF, BG,}\quad \frac{\partial \theta_{\mathrm{s}}}{\partial x} = 0 \tag{63g}$$

$$\text{along FG,}\quad \theta_{\mathrm{s}} = 1 \tag{63h}$$

$$\text{along CD,}\quad \theta_{\mathrm{f}} = 0 \tag{63i}$$

$$\text{along DE, BC,}\quad \frac{\partial \theta_{\mathrm{f}}}{\partial x} = 0 \tag{63j}$$

3.1. Interface boundary condition

Energy Eq. (59c) in the fluid is recast and written as

$$\frac{\partial \theta_{\mathrm{f}}}{\partial t} = -\left(u\frac{\partial \theta_{\mathrm{f}}}{\partial x} + v\frac{\partial \theta_{\mathrm{f}}}{\partial y}\right) + \frac{1}{RePr}\nabla^2 \theta_{\mathrm{f}} \tag{64}$$

The energy equation in the solid (59d) is recast and written as

$$\frac{\partial \theta_{\mathrm{s}}}{\partial t} = \frac{1}{RePr}\left(\frac{\partial^2 \theta_{\mathrm{s}}}{\partial x^2} + \frac{\partial^2 \theta_{\mathrm{s}}}{\partial y^2}\right) \tag{65}$$

The conjugate boundary conditions are

$$k_{\mathrm{s}}\left(\frac{\partial \theta_{\mathrm{s}}}{\partial y}\right)_{y=0} = k_{\mathrm{f}}\left(\frac{\partial \theta_{\mathrm{f}}}{\partial y}\right)_{y=0} \quad \text{and} \qquad \theta_{\mathrm{f}} = \theta_{\mathrm{s}} \quad \text{at interface } y = 0,\ 0 < x \leqslant 40 \tag{66}$$

From Taylor series expansion the flux gradients are evaluated and substituted in Eqs. (64)–(66). Simplifying, the conjugate interface temperature at next time step is,

$$\theta_{i,j}^{t+\Delta t} = \theta_{i,j}^{t} + \frac{2\Delta t}{RePr(\Delta y_{\mathrm{f}} + k\Delta y_{\mathrm{s}})} \times \left(\frac{1}{2}(\Delta y_{\mathrm{f}} + k\Delta y_{\mathrm{s}})\left(\frac{\theta_{f,i+1,j} - 2\theta_{f,i,j} + \theta_{f,i-1,j}}{\Delta x^2}\right) - k\frac{\theta_{s,i,j} - \theta_{s,i,j-1}}{\Delta y_{\mathrm{s}}} + \frac{\theta_{f,i,j+1} - \theta_{f,i,j}}{\Delta y_{\mathrm{f}}}\right)^{t} \tag{67}$$

The convergence criteria is set as sum of error from all interior points is less than 10^{-6}.

$$\sum_{i,j=1}^{i_{\max},j_{\max}} |(\theta_{i,j}^{t+\Delta t} - \theta_{i,j}^{t})|_{s,f} < \varepsilon \tag{68}$$

3.2. Grid independence study

The computational domain used has a size of 40 times the slot height in downstream direction and 20 times slot height in normal direction. To ensure that the parabolic inlet velocity profile falls exactly on the slot height, uniform grid points are used near the wall up to the slot height and beyond slot height clustered grids are used. A series of grid independence study has been done to find the optimum grid points in both directions. In x-direction the following grid systems are considered 75×49, 101×49, 125×49 and found that the average *Nu* variation is less than 1%, among the 101×49 grid points with 125×49. Further in y-direction 101×43, 101×49, 101×59, 101×67, 101×77 and

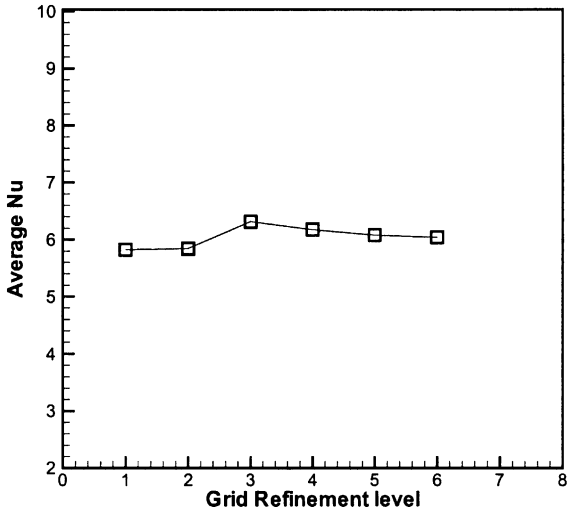

Fig. 2. Grid independence for y-direction grids: $Re = 500$, $Pr = 1.4$.

101×101 grid systems are tested (Fig. 2). It is concluded that the grid refinement level 5 (101×77) will be used for the entire calculations. In the downstream direction the clustering function used for slab is same as that of the fluid regime whereas uniform grids are used in the y-direction for both cases $\lambda = 0.25$ and $\lambda = 1$. Typical computational grids are shown in Fig. 3(a)–(c).

3.3. Validation of code

To validate the developed code, two-dimensional lid-driven square-cavity flow problem [27] and the backward-facing flow problem [28,29] have been solved. Excellent agreement has been obtained with the benchmark solutions reported in the above references. The laminar plane wall jet problem then has been solved and the computed velocity profiles are compared with the similarity solutions of Glauert [10] and the experimental results of Quintana et al. [15] in a similar way as represented by Seidel [16] (Fig. 4(a)). It is observed that at different downstream locations x/h, a good agreement amongst them has been obtained. The non-conjugate heat transfer case has been solved for $Pr = 1.4$ and 100 and compared in a similar way for five downstream locations (Fig. 4(b) and (c)).

4. Results and discussion

The present study is focused on finding a closed form relation for forced convection laminar plane wall jet as conjugate case and comparing the analytical results with numerical results. Four non-dimensional parameters (Re, Pr, λ, k) are considered for analysis. Higher complementary error function and exponential function values are evaluated using *Maple* 7.00 software [30]. For $Pr \ll 1$, it is approximated as $Pr = 0.01$ and for $Pr \geqslant 1$ it is approximated as $Pr = 100$. Results are evaluated for aspect ratios, $\lambda = 0.25$ and $\lambda = 1$, whereas thermal conductivity ratios are taken as $k = 1$, 2, 5 and 20 following Vynnycky et al. [6]. The maximum Re considered here for the study is 700, after which transition is expected [17].

For Figs. 6 and 7, different symbols are used to represent Nu and θ_b obtained by analytical results and different line patterns are used to represent the numerical results. For Fig. 8, the style is reversed.

The slab temperature contours are shown in Fig. 5(a)–(h). Results are presented for $Re(= 500)$ case. Low $Pr(= 0.01)$ and high $Pr(= 100)$ cases are considered with $k = 1$ and $k = 20$. For $Pr = 0.01$ and $k = 1$ (Fig. 5(a)), more temperature drop occurs near the inlet, than in the downstream locations. The nature of the isotherms shows that there are heat fluxes in the negative longitudinal and transverse directions near the inlet. However, there is no longitudinal variation of temperature in the downstream location signifying that only transverse variation exists. With the increases in conductivity ratio k,

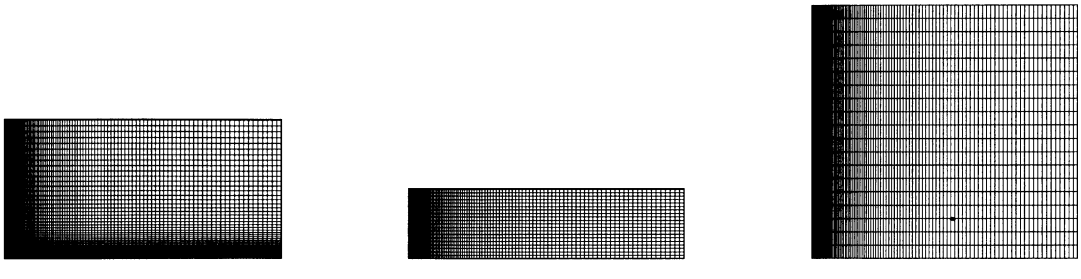

Fig. 3. Computational domain: (a) grids in the fluid regime (101×77, $\kappa = 0.7$), (b) grids in the slab regime (101×21, $\lambda = 0.25$), (c) grids in the slab regime (101×21, $\lambda = 1.0$).

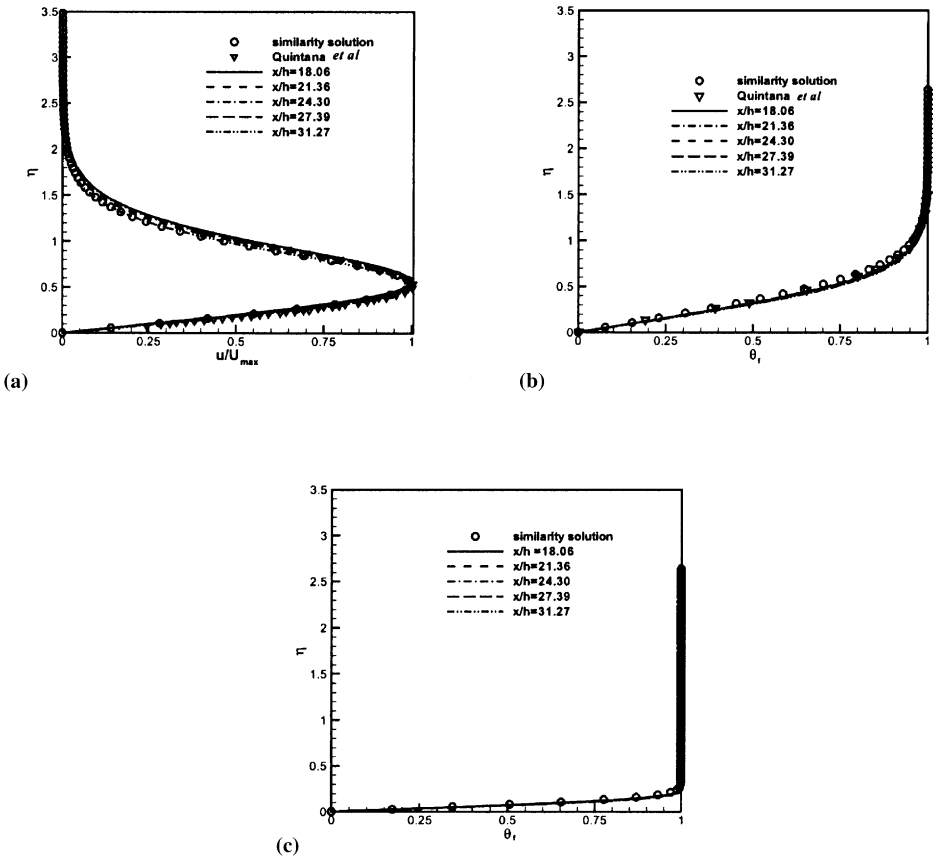

Fig. 4. Comparison of results with similarity solution for $Re = 500$: (a) comparison of horizontal velocity profile, (b) comparison of temperature profile, $Pr = 1.4$, (c) comparison of temperature profile, $Pr = 100$.

heat transfer increases across the slab and the gradient in normal direction is larger than axial direction (Fig. 5(b)), which agrees with our assumption about the conductivity of the slab. It is worthwhile to remember that if k is larger, it behaves like an isothermal slab. At high Pr, a thin thermal boundary layer develops over the interface. Most of the temperature drop occurs across the solid for both the cases. That is why the isotherm in the slab near the interface (Fig. 5(c) and (d)) has a smaller value compared to Fig. 5(a) and (b). At high Pr, the contours are less variant in the downstream direction. In other words, the temperature gradient in the longitudinal direction is much smaller than that in the transverse direction. The slab is behaving like one-dimensional heat conduction in y-direction. The isotherm plots for aspect ratio $\lambda = 1$ are shown in Fig. 5(e)–(h). For low Pr case (Fig. 5(e) and (f)), the two-dimensionality nature of the isotherms are observed. However, in the high Pr case (Fig. 5(g) and (h)), this nature is almost absent except a small region in the top-left corner.

The variations of the local Nu are shown in Fig. 6(a)–(f) for the parameters $Re = 500$, Pr=0.01,100, λ = 0.25,1.0 and for a range of k values lying between, and including, those used for Fig. 5. The numerically computed values are given for these ranges whereas the semi-analytic results are plotted for those cases where the computations are possible. At leading edge, due to large thermal gradient, Nu is greater than the rest of the length. Entrainment also causes this large gradient. The Nu comparison showed good agreement between the two methods, Fig. 6(a)–(d). Since the viscous boundary layers are dominant for high Pr fluid, the heat transfer is nearly one-dimensional (Fig. 5(c), (d), (g) and (h)) and Nu (numerical) is constant except near the leading edge. The approximation of constant-flux is expected to provide a reasonable result for $Pr \geqslant 1$ provided $k < 2$ [6]. However, as shown in Fig. 6(e)–(f), there are some discrepancies which need further investigation.

Fig. 7(a)–(d) show the non-dimensional conjugate boundary temperature for different parameters. The values considered are: $Re = 500$, $Pr = 0.01$ and 100, $\lambda = 0.25$ and 1.0, $k = 1$, 2, 5 and 20. For $Pr \ll 1$, θ_b is evaluated analytically from Eq. (44) which is a closed-form relation. The analytical results are found to be in

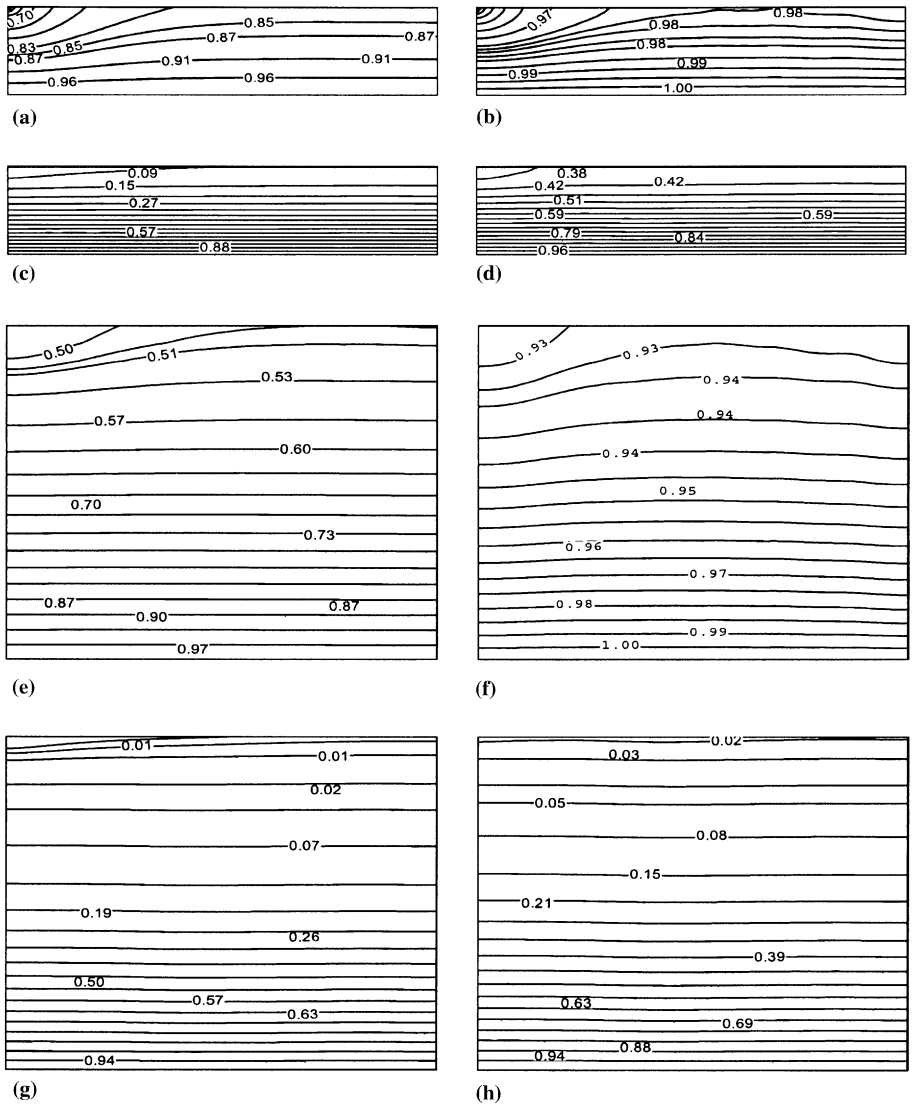

Fig. 5. Isotherm patterns within the solid slab for various parameters by numerical simulations: (a) $Re = 500$, $Pr = 0.01$, $k = 1$, $\lambda = 0.25$, (b) $Re = 500$, $Pr = 0.01$, $k = 20$, $\lambda = 0.25$, (c) $Re = 500$, $Pr = 100.0$, $k = 1$, $\lambda = 0.25$, (d) $Re = 500$, $Pr = 100.0$, $k = 20$, $\lambda = 0.25$, (e) $Re = 500$, $Pr = 0.01$, $k = 1$, $\lambda = 1.0$, (f) $Re = 500$, $Pr = 0.01$, $k = 20$, $\lambda = 1.0$, (g) $Re = 500$, $Pr = 100.0$, $k = 1$, $\lambda = 1.0$, (h) $Re = 500$, $Pr = 100.0$, $k = 20$, $\lambda = 1.0$.

very good agreement with the numerical results (Fig. 7(a) and (b)). There is some discrepancy between the analytical and computed profiles near the leading edge. It has been observed that near the inlet, the computed velocity profile differ from the similarity velocity profile due to the entrainment effect. So the discrepancy for θ_b profiles may be attributed to the above reason and the assumptions in employing the boundary conditions (Eqs. (11a) and (11b)) for the starting of the boundary layer [6]. For high Pr fluid (Fig. 7(c) and (d)), θ_b is linearly varying at leading edge. In this case, thermal boundary layer thickness is smaller than viscous boundary layer. The predicted value is closer to the numerical value at the downstream locations whereas there is some discrepancy near the leading edge. θ_b, which is related to θ_s by the uniqueness property of the Dirichlet problem, is calculated by the constant-flux approximation (Eq. (54)). The discrepancy at leading edge may be due to the presence of two-dimensionality of heat flux as shown by the isotherms (Fig. 5(c), (d), (g) and (h)).

Finally average Nusselt number dependency with Re and the comparisons with the predicted results have

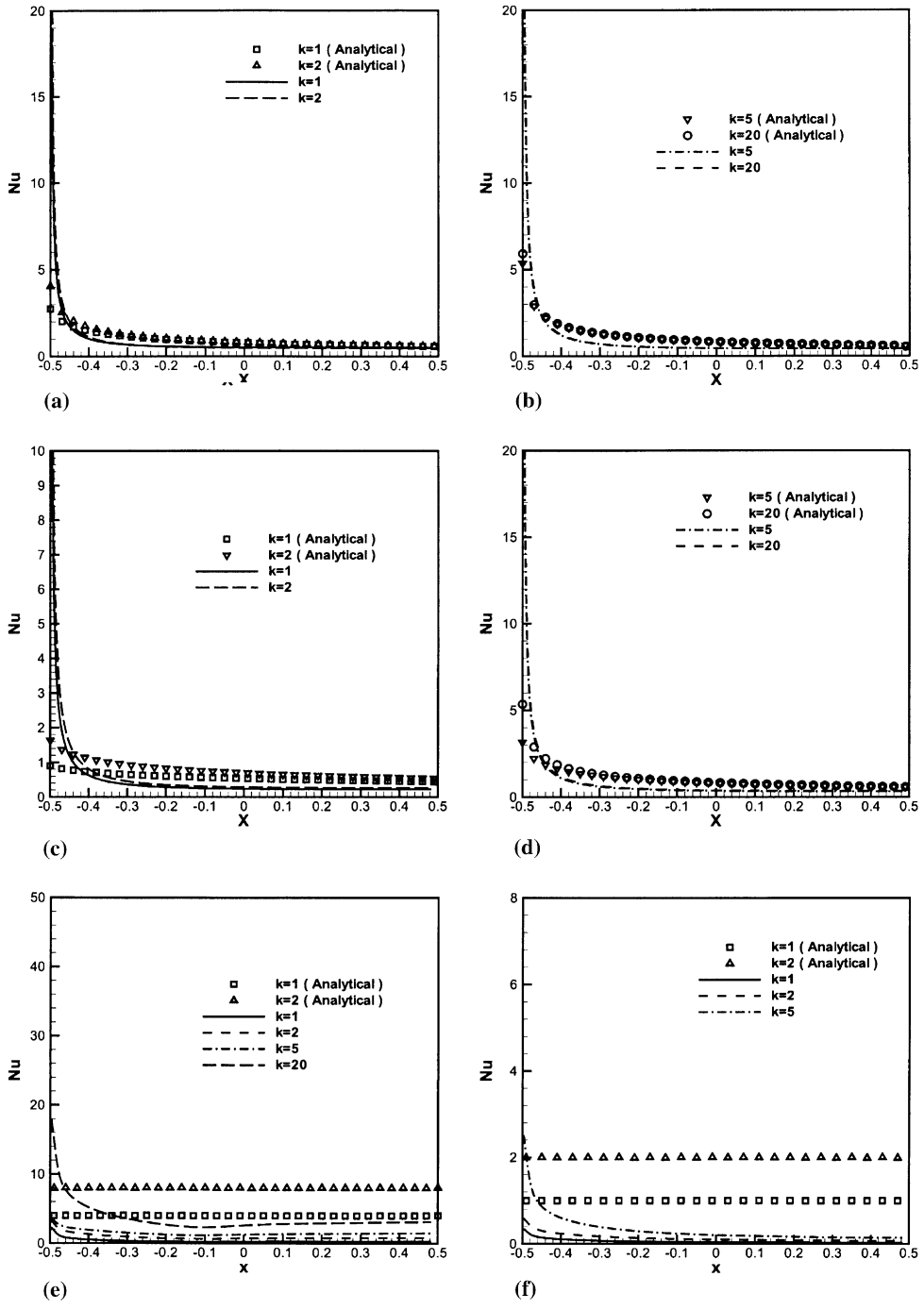

Fig. 6. Local Nusselt number (*Nu*) for different parameters: (a) $Re = 500$, $Pr = 0.01$, $\lambda = 0.25$, (b) $Re = 500$, $Pr = 0.01$, $\lambda = 0.25$, (c) $Re = 500$, $Pr = 0.01$, $\lambda = 1.0$, (d) $Re = 500$, $Pr = 0.01$, $\lambda = 1.0$, (e) $Re = 500$, $Pr = 100.0$, $\lambda = 0.25$, (f) $Re = 500$, $Pr = 100.0$, $\lambda = 1.0$.

been presented in (Fig. 8(a)–(d)). Average Nusselt number is expressed in terms of μ as given in Eq. (51). For low $Pr(= 0.01)$, there is a good agreement between the analytical and computed results (Fig. 8(a)–(b)) except at $k = 20$, $Pr = 0.01$, $\lambda = 1.0$ (Fig. 8(b)). It is found that higher aspect ratio reduces average $\overline{Nu}$. Boundary layer region becomes thinner at a higher *Re*. As expected, higher *Re* leads to higher $\overline{Nu}$ for the same λ and k values.

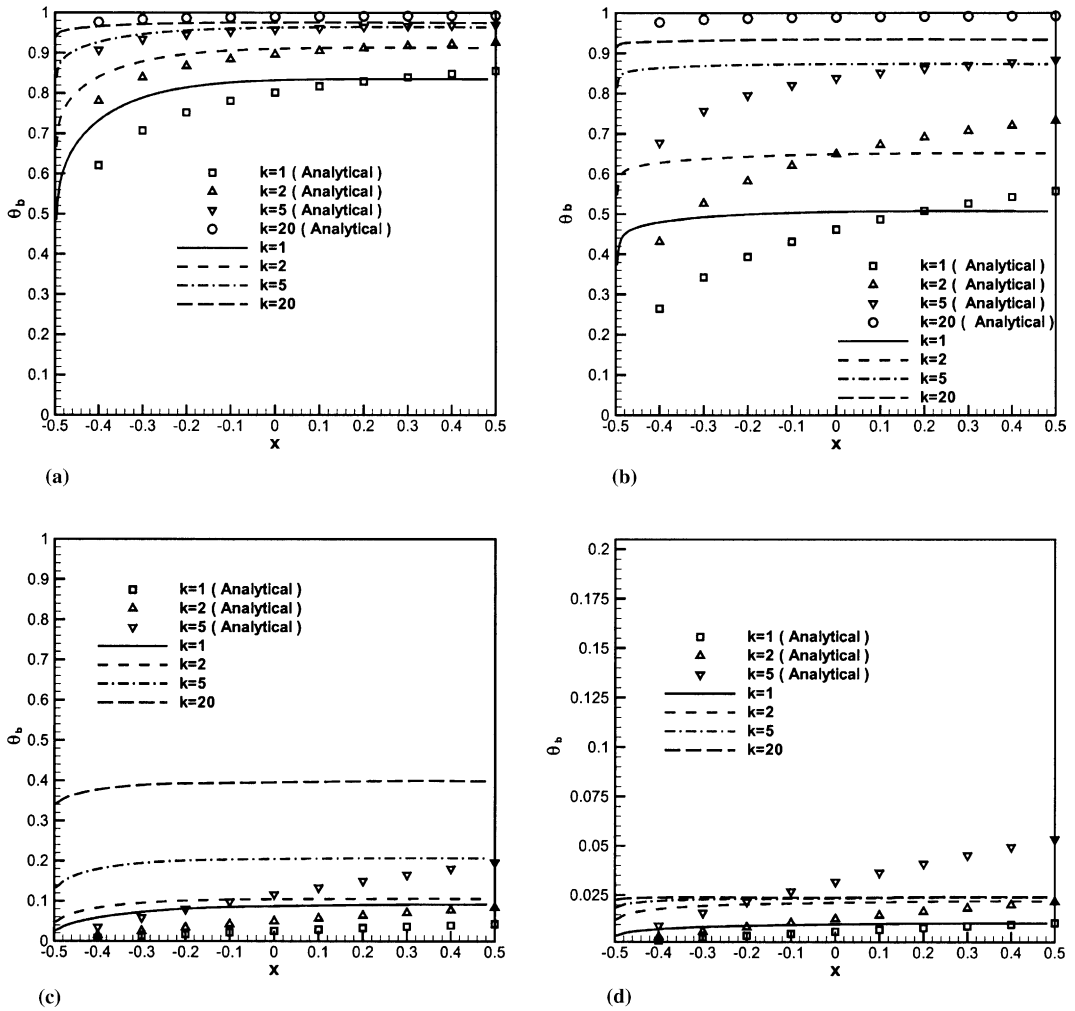

Fig. 7. Conjugate interface temperature (θ_b) for various parameters: (a) $Re = 500$, $Pr = 0.01$, $\lambda = 0.25$, (b) $Re = 500$, $Pr = 0.01$, $\lambda = 1.0$, (c) $Re = 500$, $Pr = 100.0$, $\lambda = 0.25$, (d) $Re = 500$, $Pr = 100.0$, $\lambda = 1.0$.

The difference in local Nu as discussed earlier is reflected in the average Nusselt number for high Pr. The analytical results are not matching with the numerical results for $k > 1$ which needs further investigation.

5. Conclusions

In the present work, two-dimensional laminar incompressible plane wall jet heat transfer problem has been solved analytically as well as numerically for conjugate case. Four non-dimensional parameters (Re, Pr, k, λ) are considered for analysis. Closed-form solutions have been found for local Nusselt number, conjugate boundary interface temperature and average Nusselt number. For $Pr \ll 1$, heat flow depends on $(Re^{\frac{3}{4}}Pr/k, \lambda)$ while for $Pr \geqslant 1$, the relevant parameter set is $(Re^{\frac{3}{4}}Pr^{\frac{1}{3}}/k, \lambda)$. $\bar{\theta}_b$ can be reduced, via Eq. (49), to a function of just one parameter. The governing momentum and energy equations have been solved by stream function-vorticity method treating the problem as unsteady and for a wide range of the above non-dimensional parameters. Detailed results have been reported for two cases such as $Pr \ll 1$ and $Pr \geqslant 1$. Average Nusselt number relation is found in a simple form. Singularity exists at leading edge of the conducting wall. Good agreement is found for low Pr model between the two methods. It can be said that the analytical model performs well for low Pr fluid. For high Pr fluid, analytical solution of Nusselt number relation is giving reasonable results for $k \leqslant 2$ and this needs further investigation.

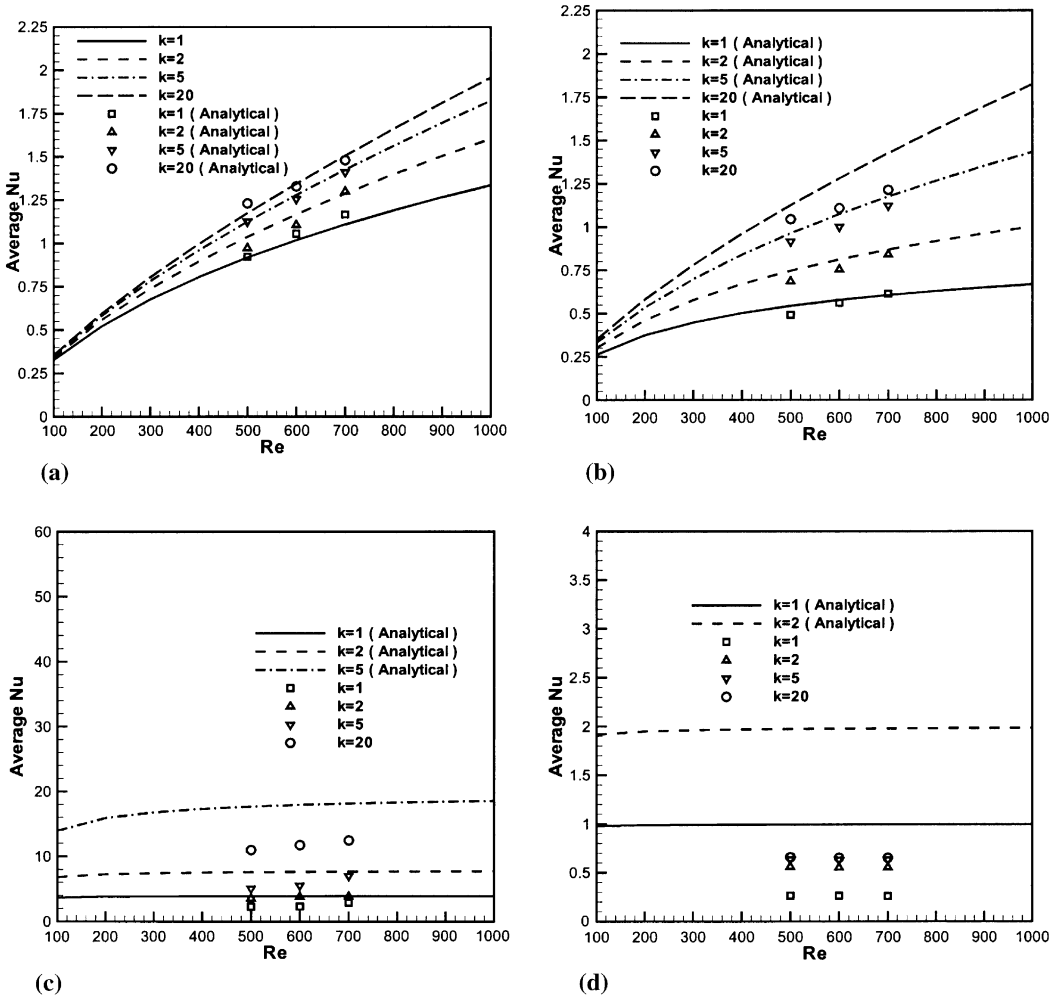

Fig. 8. Average Nusselt number for various parameters ($\overline{Nu}$): (a) $Pr = 0.01$, $\lambda = 0.25$, (b) $Pr = 0.01$, $\lambda = 1.0$, (c) $Pr = 100.0$, $\lambda = 0.25$, (d) $Pr = 100.0$, $\lambda = 1.0$.

Acknowledgements

The helpful comments of the reviewers are sincerely acknowledged by the authors.

References

[1] A. Luikov, V. Aleksashenko, A. Aleksashenko, Analytical methods of solution of conjugated problems in convective heat transfer, Int. J. Heat Mass Transfer 14 (1971) 1047–1056.

[2] A. Luikov, Conjugate convective heat transfer problems, Int. J. Heat Mass Transfer 17 (1974) 257–265.

[3] P. Payvar, Convective heat transfers to laminar flow over a plate of finite thickness, Int. J. Heat Mass Transfer 20 (1971) 431–433.

[4] I. Pop, D. Ingham, A note on conjugate forced convection boundary layer flow past a flat plate, Int. J. Heat Mass Transfer 36 (1993) 3873–3876.

[5] A. Pozzi, M. Lupo, The coupling of conduction with forced convection over a flat plate, Int. J. Heat Mass Transfer 32 (1989) 1207–1214.

[6] M. Vynnycky, S. Kimura, K. Kanev, I. Pop, Forced convection heat transfer from a flat plate: The conjugate problem, Int. J. Heat Mass Transfer 41 (1998) 45–59.

[7] W.K. Chiu, C.J. Richards, Y. Jaluria, Experimental and numerical study of conjugate heat transfer in a horizontal channel heated from below, J. Heat Transfer 123 (2001) 688–697.

[8] C. Rao, C. Balaji, S. Venkateshan, Conjugate mixed convection with surface radiation from a vertical plate with a discrete heat source, J. Heat Transfer 123 (2001) 698–702.

[9] G. Jilani, S. Jayaraj, M.A. Ahmad, Conjugate forced convection-condution heat transfer analysis of a heat

generating vertical cylinder, Int. J. Heat Mass Transfer 45 (2002) 331–341.
[10] M. Glauert, The wall jet, J. Fluid Mech. 1 (1) (1956) 1–10.
[11] W. Schwarz, B. Caswell, Some heat transfer characteristics of the two-dimensional laminar incompressible wall jet, Chem. Eng. Sci. 16 (1961) 338–351.
[12] D. Angirasa, Interaction of low-velocity plane jets with buoyant convection adjacent to heated vertical surfaces, Numer. Heat Transfer, Part A 35 (1999) 67–84.
[13] M. Amitay, J. Cohen, Instability of a two-dimensional plane wall jet, J. Fluid Mech. 344 (1997) 67–94.
[14] J. Cohen, M. Amitay, B.J. Bayly, Laminar-turbulent transition of wall-jet flows subjected to blowing and suction, Phys. Fluids 4 (1992) 283–289.
[15] D. Quintana, M. Amitay, A. Ortega, I. Wygnanski, Heat transfer in the forced laminar wall jet, J. Heat Transfer 119 (1997) 451–459.
[16] J. Seidel, Numerical investigations of forced laminar and turbulent wall jets over a heated surface, Ph.D. thesis, Faculty of the Department of Aerospace and Mechanical Engineering, The Graduate College, The University of Arizona, USA, 2001.
[17] P. Bhattacharjee, E. Loth, Simulations of laminar and transitional cold wall jets, Int. J. Heat Fluid Flow 25 (2004) 32–43.
[18] H. Schlichting, K. Gersten, Boundary Layer Theory, eighth ed., Springer, 2000, pp. 215–218.
[19] H. Carslaw, J. Jaeger, Conduction of Heat in Solids, Clarendon Press, Oxford, 1959, pp. 73–74.
[20] R. Kuyper, T.V.D. Meer, C. Hoogendoorn, R. Henkes, Numerical study of laminar and turbulent natural convection in an inclined square cavity, Int. J. Heat Mass Transfer 36 (11) (1993) 2899–2911.
[21] P.J. Roache, Fundamentals of Computational Fluid Dynamics, Hermosa, USA, 1998 (Chapter 3).
[22] G. Comini, M. Manzan, C. Nonino, Finite element solution of the stream function-voriticity equations for incompressible two-dimensional flows, Int. J. Numer. Meth. Fluids 19 (1994) 513–525.
[23] M. Napolitano, G. Pascazio, L. Quartapelle, A review of vorticity conditions in the numerical solution of the $\zeta - \psi$ equations, Comput. Fluids 28 (1999) 139–185.
[24] H. Huang, B. Wetton, Discrete compatibility in finite difference methods for viscous incompressible fluid flow, J. Comput. Phys. 126 (1996) 468–478.
[25] R. Bajura, A. Szewczyk, Experimental investigation of a laminar two-dimensional plane wall jet, Phys. Fluids 13 (1970) 1653–1664.
[26] S. Kang, R. Greif, Flow and heat transfer to a circular cylinder with a hot impinging air jet, Int. J. Heat Mass Transfer 35 (9) (1992) 2173–2183.
[27] U. Ghia, K. Ghia, C. Shin, High *Re* solutions for incompressible flow using the Navier–Stokes equations and multigrid method, J. Comput. Phys. 48 (1982) 387–411.
[28] B. Armaly, F. Durst, J. Pereira, B. Schonung, Experimental and theoretical investigation of backward-facing step flow, J. Fluid Mech. 127 (1983) 473–496.
[29] D. Gartling, A test problem for outflow boundary conditions-flow over a backward-facing step, Int. J. Numer. Meth. Fluids 11 (1990) 953–967.
[30] Maple 7.00, Waterloo Maple Inc., 2001.